Fast image scanning method in liquid-AFM without image distortion

2008 Nanotechnology 19 445701

(http://iopscience.iop.org/0957-4484/19/44/445701)

Nanotechnology **19** (2008) 445701 (8pp) doi:10.1088/0957-4484/19/44/445701

Fast image scanning method in liquid-AFM without image distortion

Inhee Choi[1], Younghun Kim[2], Jong Ho Kim[1], Young In Yang[1], Jeongjin Lee[1], Suseung Lee[1], Surin Hong[1] and Jongheop Yi[1,3]

[1] School of Chemical and Biological Engineering, Institute of Chemical Processes, Seoul National University, Seoul 151-742, Korea
[2] Department of Chemical Engineering, Kwangwoon University, Seoul 139-701, Korea

E-mail: iniini79@snu.ac.kr (I Choi), korea1@kw.ac.kr (Y Kim), jongho0@snu.ac.kr (J H Kim), netmo00@snu.ac.kr (Y I Yang), gismo97@snu.ac.kr (J Lee), jazz1863@snu.ac.kr (S Lee), pell2004@snu.ac.kr (S Hong) and jyi@snu.ac.kr (J Yi)

Received 30 May 2008, in final form 14 July 2008
Published 30 September 2008
Online at stacks.iop.org/Nano/19/445701

Abstract

High speed imaging by atomic force microscopy (AFM) allows one to directly observe the dynamic behavior of a sample surface immersed in liquid media; thus, it has been considered to be an indispensable tool for nanobiotechnology and is used in many research fields, including molecular biology and surface science. For real-time observation of a certain behavior, the high speed imaging technique should be accompanied with a high resolution imaging technique to identify target materials. To improve the image quality at a high scanning rate, we developed a variable-controlled fast scanning method, which originated from the modified squeeze–drag superposition model in liquid media. A collection of non-distorted images was accomplished after proper modification of the operating conditions in a viscous fluid, via the simple handling of loading force and cantilever length. Consequently, a speeded-up AFM imaging process was achieved in the liquid environment at up to 200 μm s^{-1}, without attachment of additional devices. The reliability of the proposed method was verified by the characterization of a grating sample immersed in three types of liquid media. In addition, the results were visualized for elastic biomolecules submerged in a liquid with high kinematic viscosity.

S Supplementary data are available from stacks.iop.org/Nano/19/445701

1. Introduction

Since 1986, when the atomic force microscope was invented as a novel microscopic tool [1], it has been extensively applied for the characterization (visualization) of various micro/nanostructures due to its image acquisition capability with high spatial resolution. This is a powerful technique for imaging macromolecules and various structures on a substrate, without regard to the sample properties (conducting or non-conducting) or imaging conditions (air or liquid), unlike other microscopic techniques such as scanning tunneling microscopy (STM), transmission electron microscopy (TEM), and scanning electron microscopy (SEM). In particular, AFM has been broadly employed in the *in situ* observation of nano/biomaterials' morphological evolution under reaction conditions because it can be readily performed in fluid [2]; thus, it is considered to be an indispensable tool for nanobiotechnology due to its high spatial resolution [3, 4]. In the early stages, high resolution image processing in liquid was achieved by operation at a slow rate [5], as compared to the scanning speed in air conditions. However, this manner of operation takes a long time to obtain an acceptable image, and limits the visualization of many interesting events that occur at much higher rates. For real-time observation of a certain behavior, a high resolution imaging technique should be accompanied with a high speed imaging technique to identify target materials. In the case of non-contact mode imaging, various efforts have been made to capture biomolecular behaviors (e.g., myosin V molecules moving on a surface) [6–11] due to its capability of imaging biological macromolecules in a nondestructive way, and since vertical oscillation of the cantilever at (or near to) its resonance

[3] Author to whom any correspondence should be addressed.

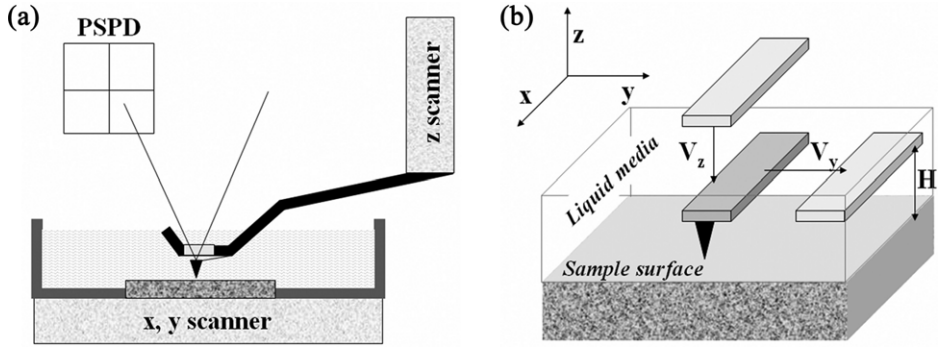

Figure 1. Schematics of a cantilever moving during tip approach with V_z and scan with V_y: (a) configuration of open liquid-cell AFM, (b) description of tip moving in liquid media during the scanning process.

frequency reduces lateral forces between the tip and the sample [12]. For this purpose, various devices have been devised by Ando *et al* [6–11], such as a high speed scanner, small cantilevers with high resonance frequencies and small spring constants, an objective lens-type of deflection detection device, and several electronic devices of wide bandwidth. The integration of these various devices was able to produce images within a few seconds, and even under a second in non-contact mode image processing. Adams *et al* [13] also developed microcantilevers with integrated piezoelectric actuators for fast imaging, which were applied to imaging bacterial cells. However, the object boundaries were obscure and their resolution was somewhat decreased when a high speed tapping mode image of *E. coli* bacteria was taken at 75.5 μm s^{-1}. In the case of contact mode imaging, Stemmer *et al* accomplished the speeding up of a scanning system by 61 μm s^{-1} for imaging plasmid DNA via an open-loop controller and feedback controller attached to a main AFM apparatus [14]. From these examples, high speed imaging in liquid has been successfully achieved by the modification of commercially available atomic force microscopes, and by attachment of accessories on the main device; however, the unique properties of the fluids were somewhat overlooked in these processes. To collect images with high spatial resolution in liquid, it is important to consider the parameters derived from the unique properties of the liquid, because AFM operation in liquid conditions is quite different from that in air condition.

Recently, we found that image distortion is correlated with the kinematic viscosity of the fluid used [5, 15]. An image scanned in a fluid with a higher kinematic viscosity has a seriously distorted result. To investigate this phenomenon, the modified squeeze–drag superposition model [15] was introduced, and thus theoretical scanning speeds for removing the effective force of the cantilever–fluid and the tip–surface were calculated. One exists near zero; the other is a much faster specific velocity. Based on this study, AFM operation in a liquid is affected by a variety of parameters unlike the operation in air, due to the large kinematic viscosity of the liquid. Importantly, the liquid properties are greatly reflected in the contact mode AFM operation, because the distance between the tip and the surface is very small in contact mode.

Here, we report on a new intelligent control method for fast image processing with high resolution that can be achieved in the contact imaging mode by controlling the experimental parameters without the attachment of modules. The contact mode is very useful for characterizing rigid materials as well as elastic materials, because simultaneous topological and frictional information can be obtained and point-administered interaction measured on the local surface during AFM operation. In this study, based on a derived theoretical formula, we propose a method that can predict the optimal scanning speed for AFM operation without image distortion. The reliability of the proposed method was demonstrated by the real characterization of a grating sample in three types of liquid media and the visualization of elastic biomolecules in liquids with high kinematic viscosity.

2. Theoretical calculations

Local fluid–substrate force interactions with resolutions in the range of piconewtons have been reported elsewhere [16, 17]. Most of the reported data are discussed in terms of the interaction ($F_{\text{net\_1}}$) between the cantilever and substrate/fluid, quantified with the tip approaching the sample in the z-direction (V_z). However, squeeze-film effects (F_{sc}) and the drag (F_{d}) on the AFM cantilevers operating in the AFM scanning process have usually been neglected. Therefore, we devised the net force acting in tip scanning ($F_{\text{net\_2}}$) in the y-direction (V_y), from the modification of $F_{\text{net\_1}}$ with the shear force for coquette flow (F_{c}) and the surface friction of the tip (F_{f}), represented by a modified squeeze–drag superposition model using the Navier–Stokes equation. This theoretical model has been described in a previous publication [15]. Here we will briefly review the principles. A schematic of the required system variables is shown in figures 1(a) and (b), and a brief explanation follows.

First, we modified the reported equations [16] for the net force ($F_{\text{net\_1}}$) acting on the tip approaching in the z-direction (V_z); the equations were modified in terms of drag force and squeeze-film force, which is considered to be the cantilever deflection during the approach of the tip to the sample.

$$F_{\text{net\_1}} = F_{\text{d}} + F_{\text{sc}} = \mu L V_z \left(\frac{4\pi}{\log\left(\frac{7.4}{Re}\right)} + \frac{3}{8S^3} \right)$$
$$= f(\mu, \rho, V_z, H) = f(\nu, V_z, H) \quad (1)$$

Table 1. Values for the parameters used in equation (2).

Parameters	Value or range	Unit	Comment
Cantilever length, L	90 (tip B) or 130 (tip C)	μm	NSC36 tip
Cantilever width, W	35	μm	NSC36 tip
Velocity, V_z or V_y	0.1 $\sim$	μm s^{-1}	Approaching or scanning
Loading force, F_n	10–90	nN	Contact mode
Tip contact area, A_t	$\pi 10^2$	nm^2	NSC36 tip
Gap between cantilever and surface, $H-15$	0.0005–1	μm	Contact to non-contact
Transition parameter, α	0–1		Dimensionless coefficient
Normalized gap, S	$\ll 1$		H/W
Viscosity, μ; density, ρ of liquid		mN s m^{-2}; g cm^{-3}	
		0.001; 1.000	Water
		1.201; 0.790	Ethanol
		2.040; 0.790	2-propanol

where Re represents the Reynolds number ($Re = \rho W V_z/\mu$) and S is a normalized gap ($S = H/W \ll 1$, where H is the gap between the tip and the surface, W is the cantilever width and L is the cantilever length, respectively). The kinematic viscosity ($\nu = \mu/\rho$) was introduced to create a one-parameter system for liquid properties (viscosity (μ) and density (ρ)).

Once the tip starts moving on the surface to obtain images, two different lateral forces are activated; the first corresponds to the force of the cantilever activated in the fluid due to the moving of the cantilever with V_y, and the second corresponds to the force of the tip activated by friction between the tip and the substrate due to the contact mode. The two activated forces are referred to as $F_{\text{cantilever-fluid}}$, and $F_{\text{tip-surface}}$, respectively. The force induced in a moving fluid intrinsically has the concept of direction, namely a vector. As shown in figure 1(b), during a scan with V_y in the y-direction, the vector direction of the friction force ($F_{\text{tip-surface}}$) between the probe tip and surface acts with one of V_y; that is, the friction force reversely acts with the scanning direction. To express the vector concept (especially direction), arrows are inserted on each term. During the scan with V_y in the y-direction, the vector direction of the friction force ($F_{\text{tip-surface}}$) acts in the opposite direction (180° reversal) to the y-component of the $F_{\text{cantilever-fluid}}$. Thus, a scalar subtraction can be denoted as follows:

$$\begin{aligned}\vec{F}_{\text{net\_2}} &= \vec{F}_{\text{cantilever\_fluid}} + \overleftarrow{F}_{\text{tip\_surface}} \\ &= \vec{F}_{\text{cantilever\_fluid}} - \vec{F}_{\text{tip\_surface}} = (F_{\text{d}} + F_{\text{sc}} + F_{\text{c}}) - F_{\text{f}} \\ &= \mu L V_y \left[\frac{4\pi}{35\log\left(\frac{7.4}{Re}\right)} + \frac{3}{4} + \frac{1}{S}\right] - \left(\frac{\mu V_y A_t}{H-15} + \alpha F_n\right) \\ &= f(\mu, \rho, V_y, H) = f(\nu, V_y, H). \end{aligned} \quad (2)$$

Consequently, the final net force ($F_{\text{net\_2}}$) during the scanning of the sample consists of forces between the cantilever–fluid and the tip–surface. Each term in equation (2) and their details have been fully elucidated in our previous work [15] and each parameter is denoted in table 1. The formula deduced for the net force ($F_{\text{net\_2}}$) is the sum of the external forces between the cantilever–fluid and the tip–surface that occurred during the scanning of the sample in liquid. Therefore, it is important to reduce the external interaction force affected by the scanning process to obtain non-distorted images. To find the optimal scanning velocity with low external interaction force during the scanning process, we solved the equation for net forces using parameters defined as in table 1.

In equation (2), we evaluated the net force ($F_{\text{net\_2}}$) for scanning in the y-direction from the introduction of the vector concept, and found two solutions for the scan rate in order to achieve zero force difference derived by the interactions of the cantilever–fluid and the tip–surface. When the scan rate approaches zero ($V_{y,0}$) or a specific velocity ($V_{y,s}$), the force of the interaction induced by the cantilever–fluid and tip–surface is reduced to a considerable extent. Scanning near a high specific velocity ($V_{y,s}$) among the two solutions is more useful and profitable for operating in liquids as compared to a low velocity ($V_{y,0}$), because it is possible to rapidly obtain a non-distorted image. Moreover, using equation (2), we determined two parameters that can directly control during image processing in certain liquid media with specific kinematic viscosities. In this study, they are the cantilever length (L) and loading force (F_n), respectively.

3. Experimental methods

3.1. Calculation of optimal scanning speed

Based on an equation (2), we developed a computer simulation program SOLFM (Scan Rate Optimization of Liquid Atomic Force Microscope; Korea program registration No. 2007-01-123-000787) that predicts the optimal scanning speed for AFM operation without image distortion. The SOLFM program was written in Microsoft Visual Basic 6.0 to implement the theory. The program can be installed and executed in the Windows operating system. This simulation was programed to find the optimal range in which the force difference ($F_{\text{net\_2}}$) enters into the stable range of 0 to ± 2 nN, where the force acting on that fluid becomes similar to that of air or water.

3.2. AFM imaging in liquid media

To verify the proposed method, scanning images by AFM were obtained for two types of sample: one is a rigid sample and the other is an elastic sample immersed in liquid media. The real characterization of a chessboard-like grating sample (TGX01, MikroMasch, Estonia) was performed in three types of liquid media: water, ethanol, and 2-propanol. Their viscosities were 0.001, 1.240 and 2.040 mN s m^{-2},

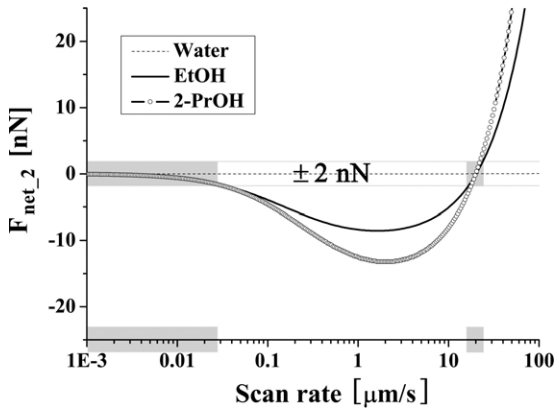

Figure 2. Net force profiles estimated by equation (2) for scanning with V_y in three types of liquid media: water, ethanol, and 2-propanol (the x-axis is represented by a logarithmic scale).

respectively. The sample was repetitively characterized under different scanning conditions as determined by the adjustment of the cantilever length and loading force. The former was conducted with two different cantilevers, B and C, and their lengths were 90 and 130 μm, respectively. The latter control method was performed at a loading force range of 10–90 nN. To demonstrate the performance of the proposed fast AFM scanning method, we also imaged elastic material in 2-propanol. As an elastic sample, *Escherichia coli* strain BL21 (DE3, Invitrogen) was selected and cultured at 37 °C and 200 rpm for 8 h in Luria–Bertani (LB) broth. The cultured bacteria cells were immobilized on a positively charged surface derived by the protonation (1 mM HCl treatment) of amine moieties on a Si surface. The amine-modified Si surface was obtained by the immersion of a 5 mM ethanolic solution of 3-aminopropyltriethoxysilane (APTES) for 3 h.

As illustrated in figure 1(a), the open liquid-cell system [2] was used in conjunction with a commercial AFM instrument (XE-100, PSIA, Korea), in order to operate in the liquids. Image distortion that is obtained with a piezoelectric tube scanner is usually due to the creep and hysteresis of the actuator. In this work, to minimize the intrinsic distortion of the apparatus, an independent z-scanner was used, which also eliminated the x–z cross-coupling problem that is inherent to conventional AFM [18–20].

4. Results

Using the proposed method, we first obtained plots in three different liquids for the net force at a fixed set-point loading force (32.55 nN for cantilever C) when the atomic force microscope was operated in air. Figure 2 shows the general behavior of the net force that escaped from the zero vicinity when the y-scan was conducted in a fluid with high kinematic viscosity. In the case of water, the force difference with the scan rate gathers near the zero point, indicating that the net force was not affected by a wide scan rate (V_y) range. That is, the low kinematic viscosity in equation (2) rarely affects the value of the net force, and thus the values exist in the zero vicinity. We demonstrate good agreement between these calculation results and the real scanning results in figure 3. At the set loading force (32.55 nN), the images were non-distorted even at a scan rate of 200 μm s^{-1}. An image resembling a chessboard that was obtained in water was almost the same as that obtained in air.

On the other hand, the force difference of the fluid with a high kinematic viscosity showed some different features as compared to that of water, and was negative below a specific y-scan rate ($V_{y,s}$). This indicates that $F_{\text{tip-surface}}$ was dominant over $F_{\text{cantilever-fluid}}$. The reverse case ($F_{\text{cantilever-fluid}}$ is dominant over $F_{\text{tip-surface}}$) was also found in the range over $V_{y,s}$. This feature became clear with an increase in the kinematic viscosity (data not shown) [15]. In the range existing between $V_{y,0}$ and $V_{y,s}$, the force difference has negative values as compared to water, and thus distorted images can result, such as tilting or blurring. Hence, when the imaging process was accomplished in viscous liquids, non-distorted images were obtained only in some specific ranges consisting of slow scan rates of 0.1 μm s^{-1} or less, and relatively fast scan rates around 30 μm s^{-1}, where the net force ($F_{\text{net\_2}}$, force difference) enters into the stable range of zero to ±2 nN, as shown in figure 2. This range reflects that the fluid becomes similar to air or water, and this was well demonstrated in the previous study [15].

Based on equation (2), these force differences, which cause image distortion, were adjusted by two parameters (L, F_n) in a certain liquid. Figures 4(a) and (b) show the results estimated for the two parameters in two liquid media, ethanol and 2-propanol, with high kinematic viscosity as described in

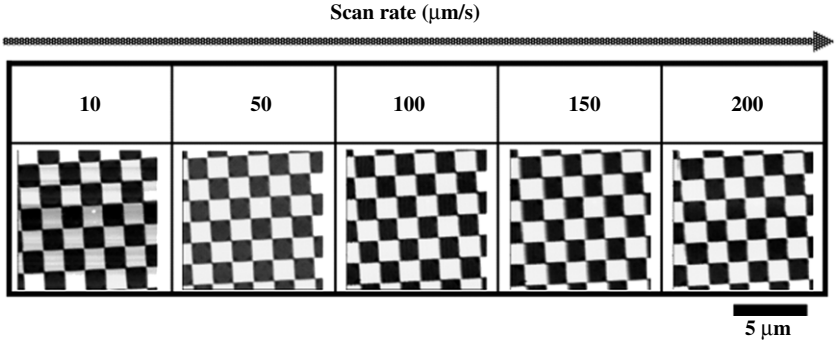

Figure 3. Images obtained at various scan rates in water (the scan area is 10 μm^2).

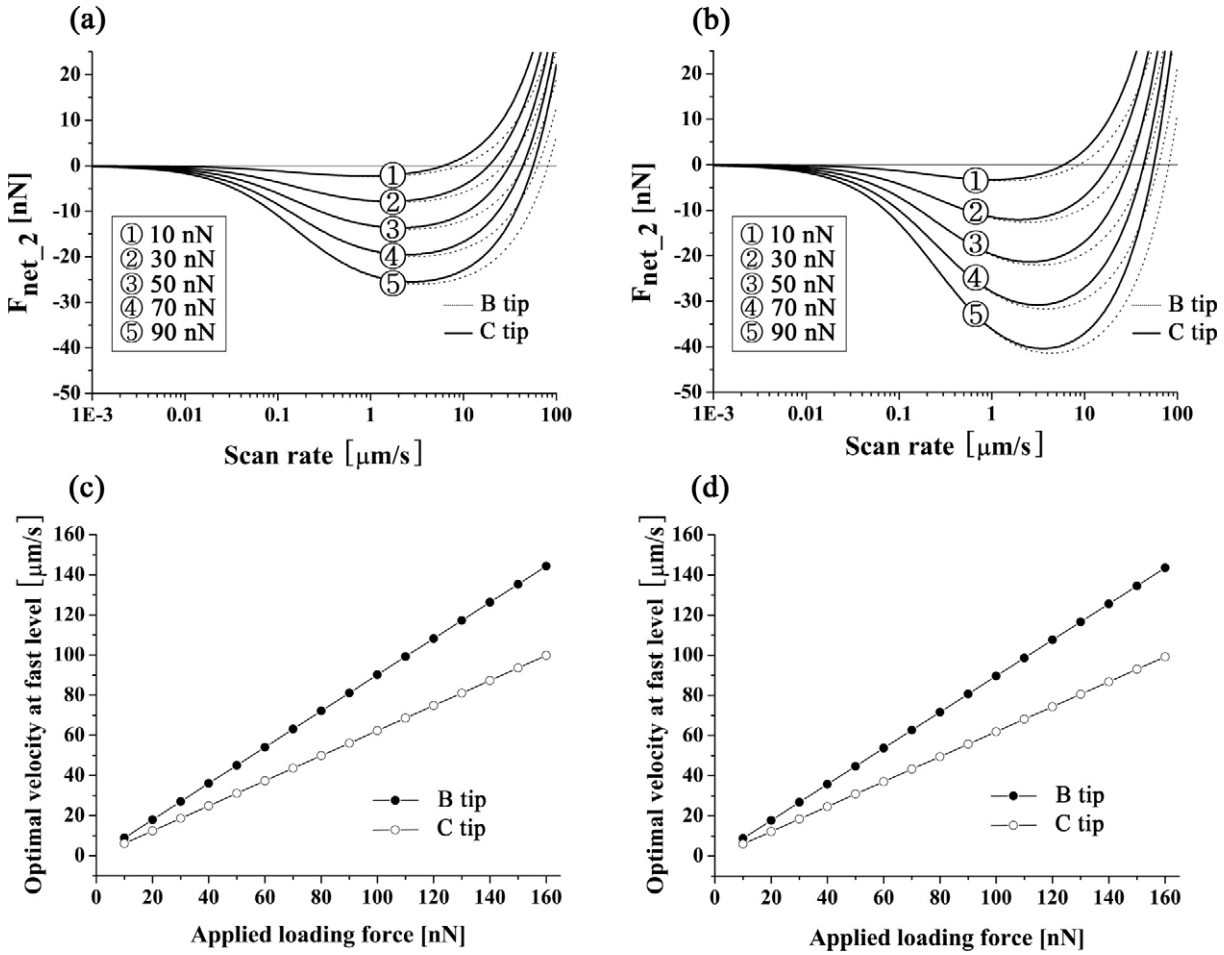

Figure 4. Net force profiles estimated by equation (2) for the two parameters of cantilever length (L) and loading force (F_n) in two liquid media with a high kinematic viscosity: (a) is for ethanol and (b) is for 2-propanol (the x-axis is represented by a logarithmic scale). Plots of optimal velocity at a fast level of applied loading force: (c) is for ethanol and (d) is for 2-propanol (near linear behavior was displayed).

table 1. As the applied loading forces gradually increased (10–90 nN), the values of $V_{y,s}$ increased dramatically. The $V_{y,s}$ values for cantilever B, of a short length, are larger than those for cantilever C, of a long length. The optimal velocity plots at a fast level of applied loading force display almost linear behavior, as shown in figures 4(c) and (d). It should be noted that non-distorted images are obtainable at a faster scanning velocity because the net force can be controlled by certain variables. When scanning was performed in the two liquids, as the loading force increased by 10 nN, the optimal scan rates also increased by about 9.0 and 6.2 μm s^{-1}, respectively, for cantilevers B and C. From the plots of figures 4(c) and (d), the linear constants have similar values irrespective of the liquids. This is due to the fact that at a set-point loading force without an additional loading force, the liquid viscosity affects both terms ($F_{\text{cantilever}-\text{fluid}}$ and $F_{\text{tip}-\text{surface}}$) of equation (2), and thus the net force reacts and changes with viscosity. However, when additional loading force was applied to the scanning process, the second term ($F_{\text{tip}-\text{surface}}$) dramatically changed with the applied loading force, and thus optimal velocity (V_y) changes followed, in order to diminish the force difference. As shown in figures 4(c) and (d), the fast optimal velocity ($V_{y,s}$) increased as the applied loading force increased. Importantly, once additional force was applied to the tip, the net force estimated by the change of kinematic viscosity had negligible values compared to the net force evaluated by the change of the loading force, due to the differential sensitivity of the variables in equation (2). Consequently, the liquid viscosity rarely affects the net force during scanning at a high loading force. The calculation results of figure 5 well demonstrate the net force profiles for the two liquids at a high loading force. Figures 5(a) and (c) show the net force profiles of the small length cantilever B and long length cantilever C, respectively. Irrespective of the liquids, the optimal velocities at the specific loading force for the two liquids were almost the same for all cases. As shown in the linear plots (see figures 5(b) and (d)) of each profile, the values of $V_{y,s}$ increase dramatically according to gradual increases of the applied loading force, and this was more effective in the case of the small length cantilever B. Because the contact area of the liquid with the cantilever becomes wider during scanning as the cantilever length increases, the first term ($F_{\text{cantilever}-\text{fluid}}$) of the net force ($F_{\text{net\_2}}$) changes with cantilever length, and thus affects the solution of equation (2). As a result, controlling the loading force and cantilever length allows synergetic effects for improving the AFM scanning

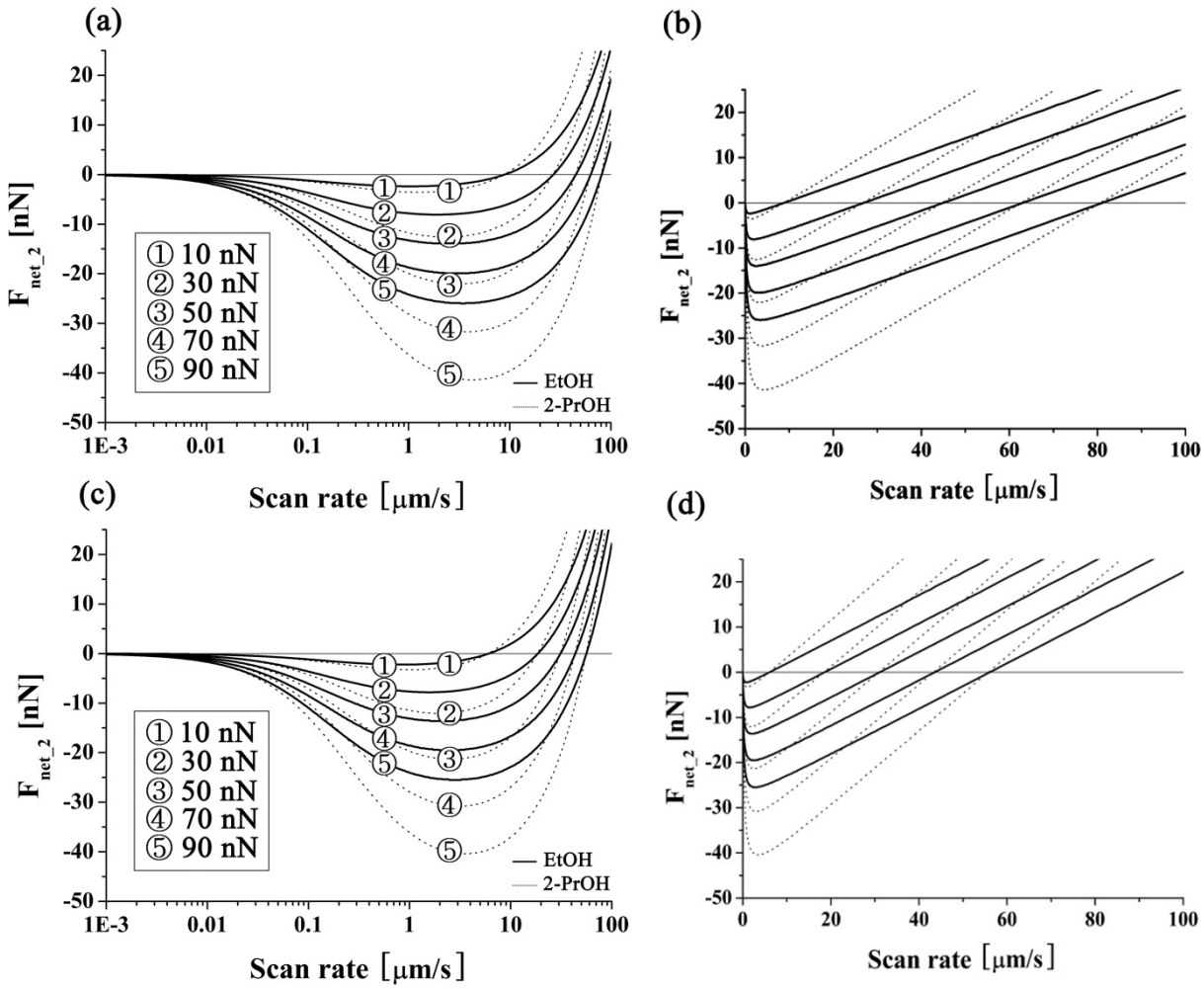

Figure 5. The net force profiles estimated by equation (2) for two liquids with increases of loading force: (a) and (b) are for the small length cantilever B and (c) and (d) are for the long length cantilever C ((a), (c): the x-axis is represented by a logarithmic scale), (b), (d): the x-axis is represented by a linear x-scale).

speed in liquids, as shown in the net force profiles of figures 4 and 5.

5. Discussion

Based on the calculated results, reduction of the force difference ($F_{\text{net\_2}}$) can be achieved by counterbalancing of the force generated by the flow of the viscous liquid during scanning; and it can be adjusted by certain variables such as the loading force (F_n) and cantilever length (L), as in this study. When the same set-point force was loaded onto the tip in both air and liquid (figure 6(a)), the tip–surface distances in liquid were greater than the tip–surface distances in air due to cantilever deflection ($F_{\text{cantilever-fluid}}$) during the approach of the tip to the sample, which is derived by the drag force and squeeze-film force in liquid media and results in image distortion. However, the increase in net force by the term $F_{\text{cantilever-fluid}}$ can be counterbalanced by applying an additional loading force, and thus the net force in liquid approaches the net force in air, as shown in the descriptions of figure 6(b). It should be noted that the operating conditions in viscous fluid can be modified to the operating conditions in non-viscous fluid via the simple handling of the loading force. This was the strategy to collect non-distorted images with fine resolution, and it was applied to the actual imaging processes of a regular grating sample and elastic bacterial cells, as proof of the model tests. The grating sample was used as a rigid sample to verify the estimated results. We collected images of the regular pattern obtained by operation with cantilever C (long) at scanning rates of 10–200 μm s^{-1} and different loading forces of 10, 32.55, and 70 nN (see S1 in the supporting information available in stacks.iop.org/Nano/19/445701). When scanning was performed at a set-point loading force (32.55 nN), the images, which were obtained at scan rates of over 20 (for ethanol) to 30 μm s^{-1} (for 2-propanol), were blurred and distorted. This distortion and blurring effect prominently occurred with scanning at a low loading force (10 nN); however, fine resolution images were gathered when fast scan rates approached 200 μm s^{-1}, as the loading force increased. This suggests that it took only several seconds to obtain a single image at this fast scanning rate (see the movie 1 of supporting data available in stacks.iop.org/Nano/19/445701). In the case of cantilever B

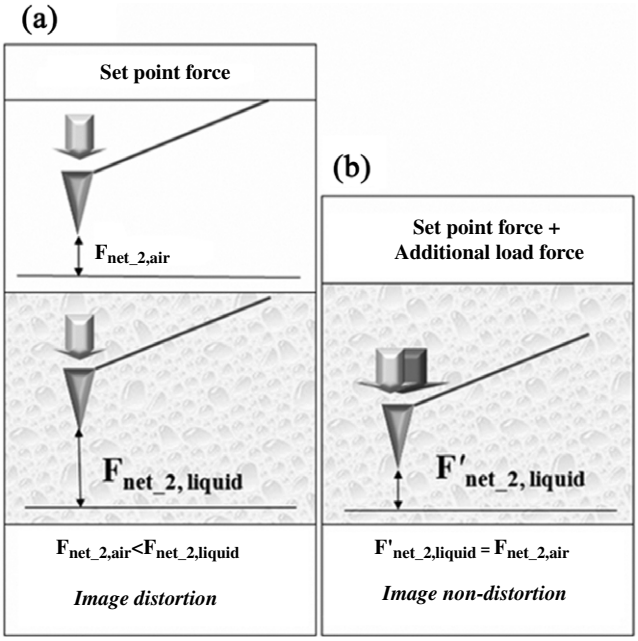

Figure 6. Description of the strategy to collect non-distorted images in highly viscous liquids: (a) when the same set-point force was loaded to the tip in the cases of both air and liquid, the tip–surface distances in liquid were greater than the tip–surface distances in air due to cantilever deflection ($F_{\text{cantilever}-\text{fluid}}$) during the approach of the tip to the sample, which is derived by drag force and squeeze-film force, and results in image distortion, (b) the net force increased by the term $F_{\text{cantilever}-\text{fluid}}$ can be counterbalanced by adding additional loading force, and thus the net force in liquid approaches the net force in air.

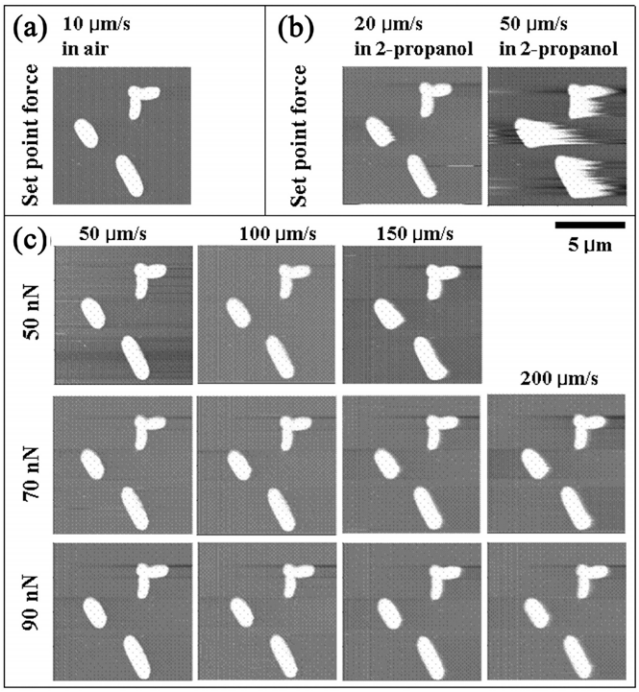

Figure 7. Comparison of the variable-controlled scanning method with the non-controlled scanning method. (a) Image characterized in air, which was carried out at a set-point loading force with a scan rate of 10 μm s^{-1}. (b) Set-point force-loaded scanning images with scan rates of 20 and 50 μm s^{-1} in 2-propanol; the images are blurred. (c) Images obtained at high speed scanning after applying the proposed method; non-distorted imaging of bacterial cells was achieved at a fast scan rate above 200 μm s^{-1} with increases of loading force. All images were obtained in 2-propanol (the scan area is 10 × 10 μm^2).

(short), the acquired images (see also S2 in the supporting information available in stacks.iop.org/Nano/19/445701) also well supported the calculated results. When scanning was performed at a set-point loading force (38.32 nN) for cantilever B, a blurring and squeezing effect was observed at the edge of the grating structure in the images, which were obtained at scan rates over an optimal velocity as estimated by simulation, about 30 (for ethanol) to 40 (for 2-propanol) μm s^{-1}, respectively. However, fine resolution images were gathered even at fast scan rates, as the loading force increased by 90 nN. When scanning was carried out at a low loading force (10 nN), a more serious blurring effect was observed in the images obtained by operation in 2-propanol rather than in ethanol. This was due to the fact that the liquid's viscosity is a measurable variable at a low loading force, as deduced in equation (2).

To examine whether the calculated results could be more widely applied to soft materials, elastic bacteria cells were characterized in 2-propanol. The morphologies of the surface-immobilized bacterial cells (figure 7(a)) were first characterized in air, which was carried out at a set-point loading force with a scan rate of 10 μm s^{-1}. After dipping into 2-propanol, the sample was further characterized at various scan rates with increased loading force. The images shown in figure 7 compare our variable-controlled scanning method with the non-controlled scanning method. By increasing the scanning rate further, the artifacts and blurring were even more pronounced in the case of the non-controlled scanning method; whereas operating the AFM by the variable-controlled scanning method resulted in images of a good quality. Set-point force-loaded scanning in 2-propanol led to image blurring (figure 7(b)); however, the image distortion at high speed scanning was overcome by the variable-controlled scanning, as shown in the captured images of figure 7(c). Consequently, the imaging of bacterial cells was achieved at fast scan rates of greater than 200 μm s^{-1} in the liquid environment.

6. Conclusions

AFM is a powerful tool for imaging macromolecules and various structures on a surface in solution. However, commercially available atomic force microscopes require several minutes to capture images, yet many interesting biological processes occur at much faster rates. Presently, AFM is limited by the speed at which it can successively record highly resolved images. Thus, we attempted to increase the scan speed of the atomic force microscope, as well as improve the image quality. It is very important to obtain non-distorted real images in liquid for applications to biological and chemical samples with nano/microstructures. For this purpose, we devised a variable-controlled high speed scanning method based on a theoretical model. To demonstrate the performance of our proposed method at high speed and to

show the improvements in image quality, we imaged a rigid grating sample and elastic bacterial cells. Consequently, we captured a 256 × 256 pixel^2 image within a few seconds via simply adjusting the scanning variables, without attaching additional tools. Although the presented results were obtained by simple control of the scanning variables, the combination of a variable-controlled scanning method with a device-aided scanning method would provide further improvements in scanning speed and image quality. This capacity offers a significant enhancement in the fast imaging for the dynamic behaviors of nano/biomaterials and the real-time imaging for the physical and chemical phenomena generated on surfaces.

Acknowledgments

This work was supported by a grant (No. R01-2006-000-10239-0) from the Basic Research Program of the Korea Science and Engineering Foundation and a Seoul National University grant of the engineering–medical multidisciplinary R&D Project. YK is grateful for the KRF grant (KRF-2007-331-D00094).

References

[1] Binnig G, Quate C F and Gerber Ch 1986 *Phys. Rev. Lett.* **56** 930
[2] Kim Y, Choi I, Kang S K, Lee J and Yi J 2006 *Rev. Sci. Instrum.* **77** 036114
[3] Giessibl F J 2005 *Mater. Today* **8** 32
[4] Giessibl F J and Quate C F 2006 *Phys. Today* **59** 44
[5] Kim Y, Kang S K, Choi I, Lee J and Yi J 2006 *Appl. Phys. Lett.* **88** 173121
[6] Ando T, Kodera N, Takai E, Maruyama D, Saito K and Toda A 2001 *Proc. Natl Acad. Sci.* **98** 12468
[7] Ando T, Kodera N, Maruyama D, Takai E, Saito K and Toda A 2002 *Japan. J. Appl. Phys.* **41** 4851
[8] Kodera N, Yamashita H and Ando T 2005 *Rev. Sci. Instrum.* **76** 053708
[9] Kodera N and Sakashita M 2006 *Rev. Sci. Instrum.* **77** 083704
[10] Ando T, Uchihashi T, Kodera N, Miyagi A, Nakakita R, Yamashita H and Sakashita M 2006 *Japan. J. Appl. Phys.* **45** 1897
[11] Uchihashi T, Kodera N, Itoh H, Yamashita H and Ando T 2006 *Japan. J. Appl. Phys.* **45** 1904
[12] Putman C A J, Van der Werf K O, De Grooth B G, Van Hulst N F and Greve J 1994 *Appl. Phys. Lett.* **64** 2454
[13] Rogers B, Sulchek T, Murray K, York D, Jones M, Manning L, Malekos S, Beneschott B and Adams J D 2003 *Rev. Sci. Instrum.* **74** 4683
[14] Schitter G, Stark R W and Stemmer A 2004 *Ultramicroscopy* **100** 253
[15] Kim Y and Yi J 2006 *J. Phys. Chem.* B **110** 20526
[16] Jones R E and Hart D P 2005 *Tribol. Int.* **38** 355
[17] Hurley C R and Leggett G J 2006 *Langmuir* **22** 4179
[18] Kwon J, Honh J, Kim Y-S, Lee D-Y, Lee S and Park S 2003 *Rev. Sci. Instrum.* **74** 4378
[19] Kim Y, Choi I, Kang S K, Lee J and Yi J 2005 *Appl. Phys. Lett.* **86** 073113
[20] Kim Y, Choi I, Kang S K, Lee J and Yi J 2006 *Appl. Phys. Lett.* **88** 013113